Two-dimensional thermodynamic theory of epitaxial $Pb(Zr,Ti)O_3$ thin films

S. Hoon Oh and Hyun M. Jang*
Department of Materials Science and Engineering and National Research Laboratory (NRL) for Ferroelectric Phase Transitions, Pohang University of Science and Technology (POSTECH), Pohang 790-784, Korea
(Received 9 February 2000; revised manuscript received 16 August 2000)

Effects of film stresses on the phase stability and various ferroelectric properties of the epitaxially oriented $Pb(Zr,Ti)O_3$ thin film were theoretically investigated. For this purpose, a two-dimensional thermodynamic model was developed using the Landau-Devonshire phenomenological theory. The theoretical computation predicts an increase in the para-ferroelectric transition temperature and an enhanced thermodynamic stability of the tetragonal-phase field, irrespective of the sign of stress (i.e., both tensile and compressive). In particular, it is predicted that tensile stress makes a new ferroelectric orthorhombic phase stable. We have also shown that dielectric properties usually exhibit their maximum values at a newly established Zr-rich morphotropic phase boundary, except for those parallel to the direction of the spontaneous polarization.

I. INTRODUCTION

The lead zirconate titanate $[Pb(Zr_{1-x}Ti_x)O_3$; PZT] solid solutions with compositions near the morphotropic phase boundary (MPB) have been widely used in various piezoelectric transducers.[1–3] The MPB of PZT system is characterized by a compositional phase boundary on which tetragonal and rhombohedral phases coexist without the solubility gap.[4] It is known that polycrystalline PZT ceramics usually exhibit their maximum values of the relative dielectric permitivity and the electromechanical coupling constant in the vicinity of the MPB.[5]

In recent years, extensive efforts have been made for the applications of PZT thin films to various modern devices. These include (i) pyroelectric IR sensors,[6] (ii) electro-optic devices,[7] (iii) surface acoustic wave (SAW) applications,[8] (iv) nonvolatile ferroelectric random access memory (FRAM) devices,[9–12] and (v) microactuators.[13,14] It is known that PZT thin films, in general, are quite different from their bulk ceramic counterparts in the microstructure and ferroelectric properties.[15–21] These differences have been attributed to (i) the presence of second phases between PZT films and substrates,[15,16] (ii) nonstoichiometric compositions,[17] (iii) residual stresses in films,[18,19] or/and (iv) surface and size effects of thin films.[20,21] Optimization of thin-film process could possibly eliminate the effects of these factors on the structure and properties of PZT thin films. However, it is very difficult, if not impossible, to remove the effects of thermal stress even in an epitaxially deposited thin film. A thermal stress in a thin film usually arises from (i) the difference in the thermal expansion coefficient between the substrate and the film, and from (ii) the difference between the working temperature and the deposition temperature.[22] Thus, a thermal stress is exerting two-dimensionally with its direction parallel to the surface of a given thin film (Fig. 1).

A stress is one of the important variables which not only influence ferroelectric properties but also affect the reliability of ferroelectric devices.[22–24] Therefore, extensive efforts have been made to theoretically understand the effects of stresses on various properties of PZT solid solutions used in modern electronics industries. However, contrary to the studies of hydrostatic stress effects on the bulk polycrystalline PZT,[25–27] few theoretical studies have been made on the effects of thin-film stresses on various properies of epitaxial PZT thin films. Recently, Oh and Jang[28] briefly examined the effects of the film stress on the phase stability of the epitaxial PZT thin film. Using the Landau-Devonshire-type thermodynamic approach, they predicted an enhanced thermodynamic stability of the tetragonal-phase field under a two-dimensional compressive stress. However, their study was limited to the epitaxial film under a compressive stress only. Furthermore, until now no one has systematically investigated the effects of the film stress on various ferroelectric properties of the epitaxial PZT thin film.

In view of these facts, the main purpose of the present study is to systematically develop a phenomenological thermodynamic theory that can be applied to PZT thin films having a wide range of compositions under both tensile (e.g., PZT/Si wafer) and compressive stresses (e.g., PZT/MgO). For this purpose, we have defined new boundary conditions relevant to various possible phases in the epitaxial PZT film, followed by the development of the elastic Gibbs functions and various theoretical relations as to ferroelectric properties. Using this approach, we have then theoretically predicted the effects of two-dimensional film stress on the thermodynamic

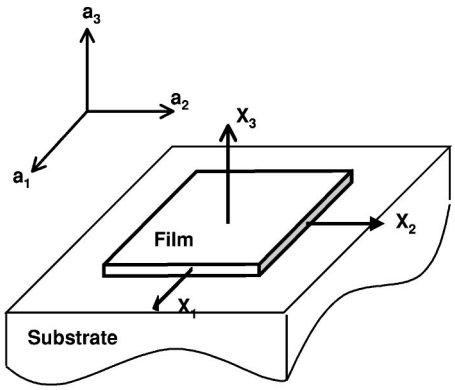

FIG. 1. Schematic representation of three normal stresses (X_1,X_2,X_3) exerted on the epitaxially oriented thin film with its crystallographic axes (a_1,a_2,a_3).

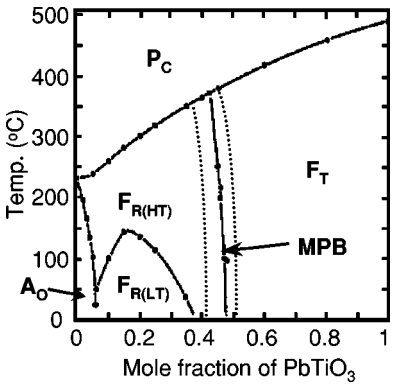

FIG. 2. Phase diagram of $PbZrO_3$-$PbTiO_3$ (PZT) solid-solution system.

stability of various relevant phases (i.e., phase diagrams) and the temperature-dependent dielectric/ferroelectric properties.

II. THEORETICAL DEVELOPMENT

The Landau-Devonshire-type phenomenological theory can be applied to investigate various properties of typical perovskite-based ferroelectrics that include $BaTiO_3$, $PbTiO_3$, and PZT. In developing phenomenological thermodynamic formalisms one has to first identify order parameters relevant to each phase transition. The PZT solid solution has various stable phase fields, depending on temperature and composition. These include paraelectric cubic (P_C), ferroelectric tetragonal (F_T), ferroelectric rhombohedral (F_R), and antiferroelectric orthorhombic (A_O) phases, as shown in the PZT phase diagram (Fig. 2). In addition to these, the rhombohedral phase is further divided into a high-temperature field ($F_{R(HT)}$) and a low-temperature one ($F_{R(LT)}$). Contrary to $F_{R(HT)}$, $F_{R(LT)}$ has a tilting or a partial rotation of the oxygen octahedron about the [111] axis of the perovskite unit cell.[27,29–31] It is known that the $F_{R(HT)}$-$F_{R(LT)}$ transition is driven by a softening of the counterclockwise oxygen rotational phonon mode.

Upon cooling, the paraelectric cubic phase undergoes a proper ferroelectric transition either to the tetragonal phase or to the high-temperature rhombohedral state, where the spontaneous polarization is the order parameter relevant to this type of transition. On the other hand, the $F_{R(HT)}$-$F_{R(LT)}$ transition is an improper ferroelectric phase transition in which a spontaneous tilting of the oxygen octahedron is the order parameter needed to describe the phase transition. In addition to these, an antiferroelectric-type polarization develops when a discontinuous transition takes place from the ferroelectric $F_{R(HT)}$ state to the antiferroelectric A_O state. In this case, therefore, the appropriate order parameter is the antiferroelectric polarization. In this study, however, we have not considered $F_{R(LT)}$ and A_O phases because the coefficients that are related to the oxygen tilt angle and the antiferroelectric polarization have not been determined yet. Because we are mainly interested in (i) the para-ferro transitions (P_C-F_T and P_C-$F_{R(HT)}$) and (ii) the tetragonal-rhombohedral (F_T-$F_{R(HT)}$) transition near the MPB, we believe that this simplification does not significantly alter our computational results.

Let us now consider the elastic Gibbs function. Based on the Landau-Devonshire phenomenological thermodynamic theory, it can be expanded[28,32] in powers of polarization and stress as

$$\begin{aligned}\Delta G=&\alpha_1(P_1^2+P_2^2+P_3^2)+\alpha_{11}(P_1^4+P_2^4+P_3^4)+\alpha_{12}(P_1^2P_2^2+P_2^2P_3^2+P_3^2P_1^2)+\alpha_{111}(P_1^6+P_2^6+P_3^6)\\&+\alpha_{112}[P_1^4(P_2^2+P_3^2)+P_2^4(P_3^2+P_1^2)+P_3^4(P_1^2+P_2^2)]+\alpha_{123}P_1^2P_2^2P_3^2-\frac{1}{2}s_{11}(X_1^2+X_2^2+X_3^2)-s_{12}(X_1X_2+X_2X_3+X_3X_1)\\&-\frac{1}{2}s_{44}(X_4^2+X_5^2+X_6^2)-Q_{11}(X_1P_1^2+X_2P_2^2+X_3P_3^2)-Q_{12}[X_1(P_2^2+P_3^2)+X_2(P_3^2+P_1^2)+X_3(P_1^2+P_2^2)]\\&-Q_{44}(X_4P_2P_3+X_5P_3P_1+X_6P_1P_2),\end{aligned}\tag{2.1}$$

where P_i and X_i are the magnitude of the polarization vector and the stress along the direction i, in accordance with the crystallographic axes of the cubic phase, α_1 is the dielectric stiffness, α_{ij}, α_{ijk} are the high-order stiffness coefficients at a constant stress, and s_{ij} are the elastic compliances measured at a constant polarization. The last three terms that contain Q_{ij} represent the electrostrictive coupling between stress and polarizations. In the reduced notation, the normal stresses are denoted by X_1, X_2, and X_3, whereas the shear stresses are denoted by X_4, X_5, and X_6. The dielectric stiffness constant, α_1, is assumed to be a linear function of temperature near the Curie point (the Curie-Weiss law). All other coefficients are assumed to be independent of temperature.[25,32] All the phenomenological coefficients were optimized by the numerical fitting of the phenomenological computations to the available experimental data for polycrystalline PZT ceramics. Their optimized values are given in a series of articles reported by Haun and co-workers.[32]

A. Boundary conditions

The first step toward the thermodynamic formulations is the establishment of suitable boundary conditions. For this purpose, we have assumed that the stress distribution over the thickness direction can be approximated by an average two-dimensional film stress.[28,33] Then, the following relations hold under this condition:

$$X_1=X_2=H,\quad X_3=X_4=X_5=X_6=0,\tag{2.2}$$

where H denotes the two normal stresses whose directions are parallel to the substrate plane or to the crystallographic axes, a_1 and a_2 (Fig. 1). A thin film is under a tensile stress if $H>0$ and under a compressive stress when $H<0$.

Let us now consider various boundary conditions that are related to the spontaneous polarization, and name these as the boundary conditions for the phase stability. Then, each relevant phase in the PZT system should satisfy the following boundary conditions for the phase stability.

Paraelectric cubic P_C:

$$P_1^2=P_2^2=P_3^2=0; \tag{2.3a}$$

Ferroelectric tetragonal F_T:

$$F_{T1}: \quad P_1^2\neq 0, \quad P_2^2=P_3^2=0, \tag{2.3b}$$

$$F_{T3}: \quad P_1^2=P_2^2=0, \quad P_3^2\neq 0; \tag{2.3c}$$

Ferroelectric orthorhombic F_O:

$$P_1^2=P_2^2\neq 0, \quad P_3^2=0; \tag{2.3d}$$

Ferroelectric rhombohedral $F_{R(HT)}$:

$$P_1^2=P_2^2\neq 0, \quad P_3^2\neq 0, \quad P_1^2\neq P_3^2. \tag{2.3e}$$

As shown in Eqs. (2.3b) and (2.3c), the ferroelectric tetragonal phase is further divided into two different fields F_{T1} and F_{T3}, depending on the direction of polarization. F_{T1} denotes the ferroelectric phase in which the polarization develops along the a_1 or a_2 direction, whereas F_{T3} designates the tetragonal phase in which the polarization is parallel to the a_3 direction (Fig. 1). It is known that the ferroelectric orthorhombic phase, F_O, is not stable under the condition of zero stress. We have included the boundary condition for F_O because a stress in a thin film can possibly make the orthorhombic phase F_O stable. The three polarization vectors are generally equal in their magnitudes in the ferroelectric rhombohedral phase $F_{R(HT)}$. Under the condition of two-dimensional stress, however, it is expected that they are not equal to each other, as given in Eq. (2.3e).

B. Elastic Gibbs functions

We are now in a position to derive various relations as to ferroelectric properties starting from a generic form of the elastic Gibbs function given in Eq. (2.1). Applying various boundary conditions summarized in Eqs. (2.2) and (2.3) to Eq. (2.1), one can obtain the following expressions for the elastic Gibbs functions.

Paraelectric cubic P_C:

$$\Delta G=-(s_{11}+s_{12})H^2; \tag{2.4a}$$

Ferroelectric tetragonal F_T:

$$F_{T1}: \quad \Delta G=-(s_{11}+s_{12})H^2+[\alpha_1-(Q_{11}+Q_{12})H]P_1^2 + \alpha_{11}P_1^4+\alpha_{111}P_1^6, \tag{2.4b}$$

$$F_{T3}: \quad \Delta G=-(s_{11}+s_{12})H^2+(\alpha_1-2Q_{12}H)P_3^2+\alpha_{11}P_3^4 + \alpha_{111}P_3^6; \tag{2.4c}$$

Ferroelectric orthorhombic F_O:

$$\Delta G=-(s_{11}+s_{12})H^2+2[\alpha_1-(Q_{11}+Q_{12})H]P_1^2 + (2\alpha_{11}+\alpha_{12})P_1^4+2(\alpha_{111}+\alpha_{112})P_1^6; \tag{2.4d}$$

Ferroelectric rhombohedral $F_{R(HT)}$:

$$\begin{aligned}\Delta G=&-(s_{11}+s_{12})H^2+\alpha_1(2P_1^2+P_3^2)+\alpha_{11}(2P_1^4+P_3^4)\\ &+\alpha_{12}(P_1^2+2P_3^2)P_1^2+\alpha_{111}(2P_1^6+P_3^6)\\ &+2\alpha_{112}(P_1^6+P_1^4P_3^2+P_1^2P_3^4)+\alpha_{123}P_1^4P_3^2\\ &-2Q_{11}P_1^2H-2Q_{12}(P_1^2+P_3^2)H.\end{aligned} \tag{2.4e}$$

C. Spontaneous polarization

Various expressions for the spontaneous polarization can be derived from the elastic Gibbs functions using the stability criterion of the first partial derivative ($\partial\Delta G/\partial P_i=0$), as shown below.

Paraelectric cubic P_C:

$$P_3^2=0; \tag{2.5a}$$

Ferroelectric tetragonal F_T:

$$F_{T1}: \quad P_1^2=\frac{-\alpha_{11}+\sqrt{\alpha_{11}^2-3\alpha_{111}[\alpha_1-(Q_{11}+Q_{12})H]}}{3\alpha_{111}}, \tag{2.5b}$$

$$F_{T3}: \quad P_3^2=\frac{-\alpha_{11}+\sqrt{\alpha_{11}^2-3\alpha_{111}(\alpha_1-2Q_{12}H)}}{3\alpha_{111}}; \tag{2.5c}$$

Ferroelectric orthorhombic F_O:

$$P_1^2=\frac{-(2\alpha_{11}+\alpha_{12})+\sqrt{(2\alpha_{11}+\alpha_{12})^2-12(\alpha_{111}+\alpha_{112})[\alpha_1-(Q_{11}+Q_{12})H]}}{6(\alpha_{111}+\alpha_{112})}; \tag{2.5d}$$

Ferroelectric rhombohedral $F_{R(HT)}$:

$$P_3^2=\frac{-(\alpha_{11}+2\alpha_{112}P_1^2)+\sqrt{(\alpha_{11}+2\alpha_{112}P_1^2)^2-3\alpha_{111}[\alpha_1-2Q_{12}H+(2\alpha_{112}+\alpha_{123})P_1^4+2\alpha_{12}P_1^2]}}{3\alpha_{111}}; \tag{2.5e}$$

$$P_1^2=-\frac{2\alpha_{11}+\alpha_{12}+2\alpha_{112}P_3^2+\alpha_{123}P_3^2}{6(\alpha_{111}+\alpha_{112})} + \frac{\sqrt{(2\alpha_{11}+\alpha_{12}+2\alpha_{112}P_3^2+\alpha_{123}P_3^2)^2-12(\alpha_{111}+\alpha_{112})[\alpha_1-(Q_{11}+Q_{12})H+\alpha_{112}P_3^4+\alpha_{12}P_3^2]}}{6(\alpha_{111}+\alpha_{112})}. \tag{2.5f}$$

In case of the rhombohedral phase, P_1 and P_3 could be obtained, in principle, by simultaneously solving two self-consistent equations, as given in Eqs. (2.5e) and (2.5f). However, we were not able to obtain analytical expressions for P_1 and P_3. Therefore, we have employed the Newton's numerical method to obtain these.

D. Dielectric properties

Various expressions for the reciprocal relative dielectric susceptibility (relative dielectric stiffness, χ_{ij}) can be derived using the boundary conditions given in Eqs. (2.2) and (2.3) and the second partial derivative of the free energy function $\chi_{ij}(=\varepsilon_0\partial^2\Delta G/\partial P_i\partial P_j)$, where ε_0 is the dielectric permittivity of free space. The results for each relevant phase are summarized below.

Paraelectric cubic P_C:

$$\chi_{11}=\chi_{22}=2\varepsilon_0[\alpha_1-(Q_{11}+Q_{12})H],$$
$$\chi_{33}=2\varepsilon_0(\alpha_1-2Q_{12}H),$$
$$\chi_{12}=\chi_{23}=\chi_{31}=0; \tag{2.6a}$$

Ferroelectric tetragonal F_T:

F_{T1}:

$$\chi_{11}=2\varepsilon_0[\alpha_1+6\alpha_{11}P_1^2+15\alpha_{111}P_1^4-(Q_{11}+Q_{12})H],$$
$$\chi_{22}=2\varepsilon_0[\alpha_1+\alpha_{12}P_1^2+\alpha_{112}P_1^4-(Q_{11}+Q_{12})H],$$
$$\chi_{33}=2\varepsilon_0(\alpha_1+\alpha_{12}P_1^2+\alpha_{112}P_1^4-2Q_{12}H),$$
$$\chi_{12}=\chi_{23}=\chi_{31}=0; \tag{2.6b}$$

F_{T3}:

$$\chi_{11}=\chi_{22}=2\varepsilon_0[\alpha_1+\alpha_{12}P_3^2+\alpha_{112}P_3^4-(Q_{11}+Q_{12})H],$$
$$\chi_{33}=2\varepsilon_0(\alpha_1+6\alpha_{11}P_3^2+15\alpha_{111}P_3^4-2Q_{12}H),$$
$$\chi_{12}=\chi_{23}=\chi_{31}=0; \tag{2.6c}$$

Ferroelectric orthorhombic F_O:

$$\chi_{11}=\chi_{22}=2\varepsilon_0[\alpha_1+(6\alpha_{11}+2\alpha_{12})P_1^2 + (15\alpha_{111}+7\alpha_{112})P_1^4-(Q_{11}+Q_{12})H],$$
$$\chi_{33}=2\varepsilon_0(\alpha_1+2\alpha_{12}P_1^2+(2\alpha_{111}+\alpha_{123})P_1^4-2Q_{12}H),$$
$$\chi_{12}=4\varepsilon_0(\alpha_{12}P_1^2+4\alpha_{112}P_1^4), \quad \chi_{23}=\chi_{31}=0; \tag{2.6d}$$

Ferroelectric rhombohedral $F_{R(HT)}$:

$$\chi_{11}=\chi_{22}=2\varepsilon_0[\alpha_1+(6\alpha_{11}+\alpha_{12})P_1^2+(15\alpha_{111}+7\alpha_{112})P_1^4 + (6\alpha_{112}+\alpha_{123})P_1^2P_3^2+\alpha_{12}P_3^2+\alpha_{112}P_3^4 - (Q_{11}+Q_{12})H],$$
$$\chi_{33}=2\varepsilon_0[\alpha_1+2\alpha_{12}P_1^2+(2\alpha_{112}+\alpha_{123})P_1^4+12\alpha_{112}P_1^2P_3^2 + 6\alpha_{11}P_3^2+15\alpha_{111}P_3^4-2Q_{12}H],$$
$$\chi_{12}=4\varepsilon_0(\alpha_{12}P_1^2+4\alpha_{112}P_1^4+\alpha_{123}P_1^2P_3^2),$$
$$\chi_{23}=\chi_{31}=4\varepsilon_0[\alpha_{12}P_1P_3+(2\alpha_{112}+\alpha_{123})P_1^3P_3 + 2\alpha_{112}P_1P_3^3]. \tag{2.6e}$$

The dielectric susceptibility coefficients η_{ij} can be determined from the reciprocal of the dielectric stiffness matrices χ_{ij} as follows.

Paraelectric cubic P_C:

$$\eta_{11}=\eta_{22}=1/\chi_{11}, \quad \eta_{33}=1/\chi_{33},$$
$$\eta_{12}=\eta_{23}=\eta_{31}=0; \tag{2.7a}$$

Ferroelectric tetragonal F_T:

F_{T1}:

$$\eta_{11}=1/\chi_{11}, \quad \eta_{22}=1/\chi_{22}, \quad \eta_{33}=1/\chi_{33},$$
$$\eta_{12}=\eta_{23}=\eta_{31}=0; \tag{2.7b}$$

F_{T3}:

$$\eta_{11}=\eta_{22}=1/\chi_{11}, \quad \eta_{33}=1/\chi_{33},$$
$$\eta_{12}=\eta_{23}=\eta_{31}=0; \tag{2.7c}$$

Ferroelectric orthorhombic F_O:

$$\eta_{11}=\eta_{22}=\chi_{11}/(\chi_{11}^2-\chi_{12}^2), \quad \eta_{33}=1/\chi_{33},$$
$$\eta_{12}=-\chi_{12}/(\chi_{11}^2-\chi_{12}^2), \quad \eta_{23}=\eta_{31}=0; \tag{2.7d}$$

Ferroelectric rhombohedral $F_{R(HT)}$:

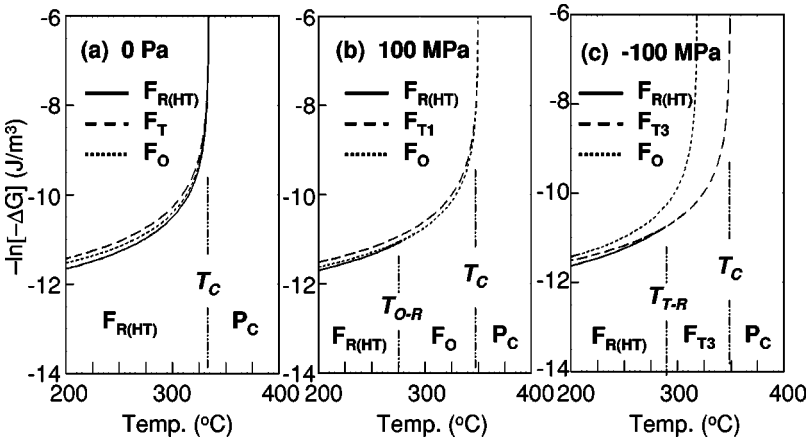

FIG. 3. Elastic Gibbs free energy of tetragonal, orthorhombic, and rhombohedral phases plotted as a function of temperature for the PZT 70/30 (Zr/Ti=70/30) at three different values of two-dimensional stress: (a) 0 Pa, (b) 100 MPa, and (c) −100 MPa.

$$\eta_{11}=\eta_{22}=\frac{\chi_{13}^2-\chi_{11}\chi_{33}}{(\chi_{11}-\chi_{12})[2\chi_{13}^2-(\chi_{11}+\chi_{12})\chi_{33}]},$$

$$\eta_{33}=\frac{-(\chi_{11}+\chi_{12})}{2\chi_{13}^2-(\chi_{11}+\chi_{12})\chi_{33}},$$

$$\eta_{12}=\frac{-\chi_{13}^2+\chi_{12}\chi_{33}}{(\chi_{11}-\chi_{12})[2\chi_{13}^2-(\chi_{11}+\chi_{12})\chi_{33}]},$$

$$\eta_{23}=\eta_{31}=\frac{\chi_{13}}{2\chi_{13}^2-(\chi_{11}+\chi_{12})\chi_{33}}. \tag{2.7e}$$

The above relative dielectric susceptibility coefficients are based on the three crystallographic axes of the cubic P_{m3m} symmetry. Dielectric susceptibilities, in general, are expressed as values according to the polar directions. Therefore, for orthorhombic and rhombohedral phases, new susceptibility coefficients are needed because the directions of polarization, in these cases, are not parallel to those for the original cubic axes. However, in case of the rhombohedral state, the newly formed dielectric susceptibility coefficients are extremely complicated to handle because the magnitude of polarization vector depends on the direction (i.e., $P_1^2=P_2^2\neq P_3^2$) under a two-dimensional stress. Therefore, in this study, we have examined various ferroelectric properties using the dielectric susceptibility coefficients obtained from the original cubic axes.

III. RESULTS AND DISCUSSION

In this section, we will present various computational results related to the phase stability and ferroelectric properties of the epitaxial PZT thin film. For this purpose, we have used various equations derived in Sec. II and the phenomenological coefficients reported in the literature.[32] The ferroelectric properties that we have examined include the elastic Gibbs free energy, the spontaneous polarization, and the dielectric susceptibility. For the purpose of comparison, we have chosen the PZT systems having two different compositions with Zr/Ti=70/30 and 30/70. In the absence of stress, the former (i.e., Zr/Ti=70/30) corresponds to the rhombohedral phase while the latter belongs to the stable tetragonal-phase field.

A. Phase diagram

The presence of film stress may strongly affect the thermodynamic stability of various phases involved. Therefore, it is useful to systematically examine the effect of the nature (or sign) of film stress on the stability of each relevant phase for a wide range of temperature. In Figs. 3 and 4, the elastic Gibbs free energies are plotted as a function of temperature for three different stress states. In case of the tetragonal phase, we have plotted the results only for the more stable phase among the two possible states, F_{T1} and F_{T3}. Certainly, the free energies of both states are equal to each other (degenerate) in the absence of stress. The effects of the two-dimensional film stress on the elastic Gibbs free energy of the PZT 70/30 (Zr/Ti=70/30) are summarized in Fig. 3. In the absence of stress, the rhombohedral phase has the lowest

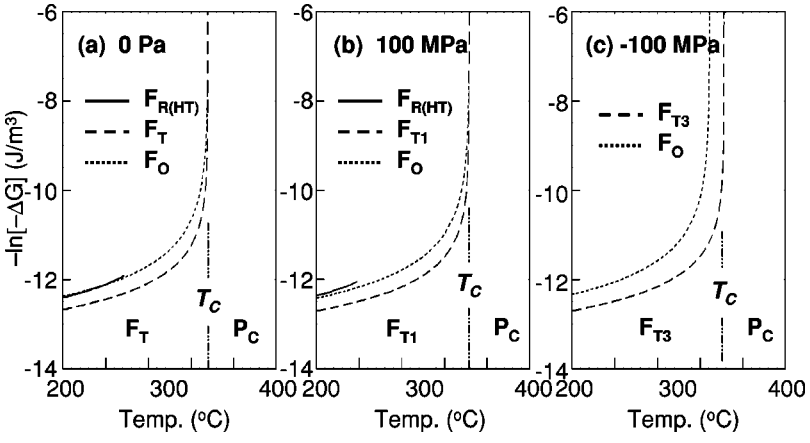

FIG. 4. Elastic Gibbs free energy of tetragonal, orthorhombic, and rhombohedral phases plotted as a function of temperature for the PZT 30/70 (Zr/Ti=30/70) at three different values of two-dimensional stress: (a) 0 Pa, (b) 100 MPa, and (c) −100 MPa.

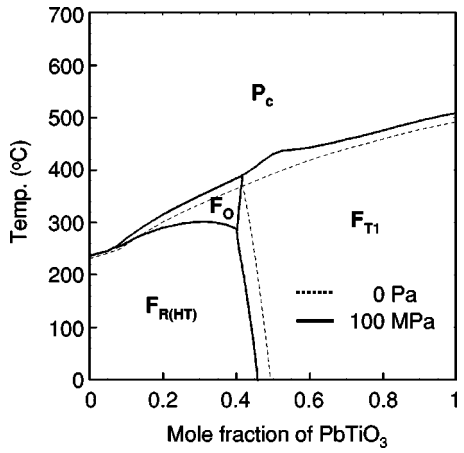

FIG. 5. The computed phase diagram of $PbZrO_3$-$PbTiO_3$ (PZT) pseudobinary system, showing the effect of two-dimensional tensile stress on the stable phase field. The dotted lines represent the phase boundaries in the absence of stress. On the other hand, the solid lines correspond to those under a tensile stress of 100 MPa.

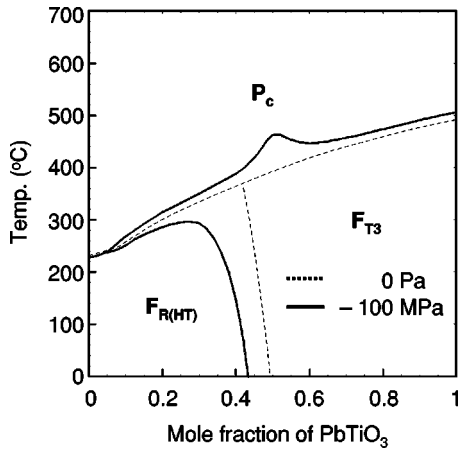

FIG. 6. The computed phase diagram of $PbZrO_3$-$PbTiO_3$ (PZT) pseudobinary system, showing the effect of two-dimensional compressive stress on the shift of stable phase boundaries. The dotted lines represent the phase boundaries in the absence of stress. On the other hand, the solid lines correspond to those under a compressive stress of -100 MPa.

free energy for temperatures below the Curie point T_C and, thus, is the stable state. This is consistent with the conclusion drawn from the experimental phase diagram presented in Fig. 2. As shown in Fig. 3(b), the para-ferro transition point (T_C) increases and the ferroelectric orthorhombic phase becomes the stable phase field between $T_{O\text{-}R}$ and T_C in the presence of tensile stress. It is expected that the presence of tensile stress expedites the polarization to align along the a_1 or a_2 direction. In the presence of compressive stress, the para-ferro transition point (T_C) also increases but the tetragonal F_{T3} phase now becomes the stable phase between $T_{T\text{-}R}$ and T_C, as shown in Fig. 3(c). It is expected that the compressive stress promotes the spontaneous polarization to be oriented along the a_3 direction or perpendicular to the substrate plane. Thus the F_{T3} phase becomes stable with increasing compressive stress.

Figure 4 presents the elastic Gibbs free energy of the Ti-rich PZT 30/70 as a function of temperature. Irrespective of the sign, the presence of film stress increases the Curie temperature slightly, and the tetragonal phase is the stable phase field below T_C. The computational results further indicate that the stability of F_{T1} is enhanced by the presence of tensile film stress while the tetragonal F_{T3} is stabilized under a compressive stress. This is because the polarization is likely to align along the direction of tensile stress.

The computed phase diagrams of the epitaxial PZT thin film under two-dimensional tensile and compressive stresses are respectively presented in Figs. 5 and 6. For the identification of phase boundary, we have used the fact that a phase transition occurs whenever two lowest free energy curves intersect each other. The dotted lines represent the phase boundaries in the absence of stress while the solid lines correspond to those under a two-dimensional stress. As shown in the figures, irrespective of the sign of film stress, the Curie temperature increases and the tetragonal-rhombohedral transition points (the MPB) move toward the rhombohedral-phase field under a two-dimensional film stress. One of the prominent features of the simulated phase diagram under a tensile stress is the appearance of the stable orthorhombic-phase field. The simulated result thus predicts a possibility of the existence of a new ferroelectric orthorhombic phase before it is experimentally identified.

To experimentally test our theoretical predictions, we have estimated the cubic-tetragonal transition temperature of the epitaxial PZT 30/70 film (thickness 200 nm) on a MgO (001) substrate using the method of differential thermal analysis (DTA; Perkin Elmer DTA-7). In addition to this, we have separately prepared a high-purity sol-gel-derived PZT 30/70 powder and measured the transition temperature in the absence of any stress. The transition point of the PZT 30/70 film on MgO was 470 °C (cooling cycle). The difference in the transition temperature between these two PZT samples was slightly larger than 30°, suggesting that the compressive thermal stress developed in the film was larger than 100 MPa (Fig. 6) for temperatures above the transition point. XRD analysis further indicated that the film was highly *c*-axis oriented for the thickness up to 200 nm. This indicates that the F_{T3} phase is stable below the cubic-tetragonal transition temperature, and is consistent with the theoretical prediction as presented in Fig. 6. From these experimental observations one can conclude that the displacive P_C-F_{T3} phase transition temperature of the PZT 30/70 film on a MgO (001) substrate is substantially higher than the transition point of the stress-free PZT 30/70 powder.

According to our detailed theoretical estimates, the Zr/Ti ratio should be greater than 60/40 for the fabrication of the epitaxial PZT film in which tetragonal and rhombohedral phases coexist (abbreviated as the MPB PZT film). This ratio significantly deviates from the bulk MPB composition (Zr/Ti=52/48). Therefore, our computations, partly presented in Figs. 5 and 6, adequately explain the observed difficulty in the fabrication of the MPB PZT film using a film composition in the vicinity of the bulk MPB. Based on all these theoretical arguments, we have recently fabricated the epitaxial MPB PZT film using the Zr/Ti ratio greater 60/40, supporting our theoretical prediction. A more detailed discussion on the fabrication of the epitaxial MPB PZT film will be given in a forthcoming paper.

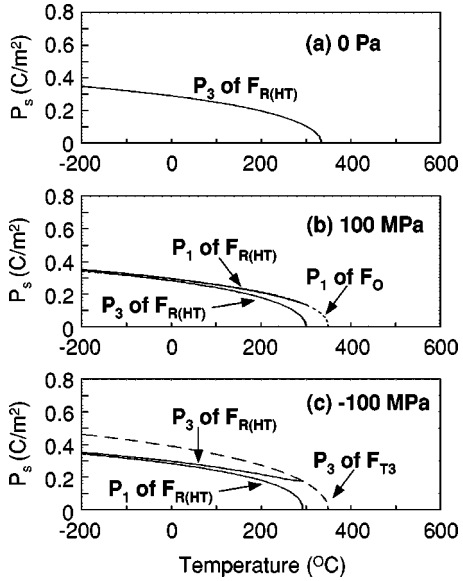

FIG. 7. Simulated spontaneous polarization of the PZT 70/30 vs temperature at three different values of two-dimensional stress. (a) 0 Pa, (b) 100 MPa, and (c) −100 MPa.

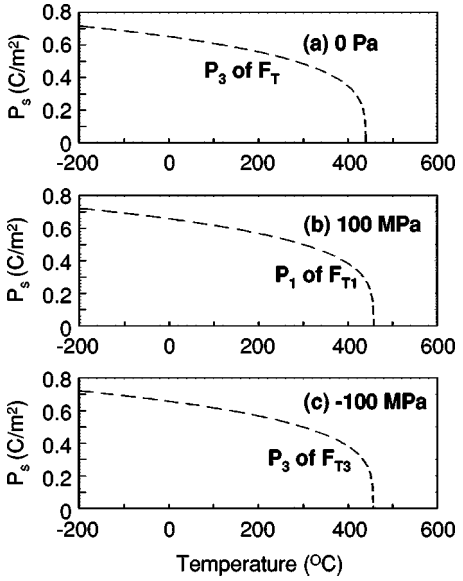

FIG. 8. Simulated spontaneous polarization of the PZT 30/70 vs temperature at three different values of two-dimensional stress: (a) 0 Pa, (b) 100 MPa, and (c) −100 MPa.

B. Spontaneous polarization

Let us now examine the simulated spontaneous polarization as a function of temperature. The effects of the two-dimensional film stress on the temperature-dependent spontaneous polarization of the Zr-rich PZT 70/30 epitaxial thin film are summarized in Fig. 7. As shown in the figure, the presence of two-dimensional film stress, irrespective of the sign, increases the para-ferroelectric transition temperature. However, phase transition characteristics are not significantly influenced by the presence and the sign of film stress. Under a tensile stress, the spontaneous polarization P_1 associated with the formation of the orthorhombic phase F_O first appears at the Curie temperature, and the polarization increases until the orthorhombic phase, F_O, transforms to the rhombohedral phase, $F_{R(HT)}$. Under a compressive stress, on the other hand, the spontaneous polarization P_3 of the tetragonal phase, F_{T3}, occurs first upon cooling from the paraelectric state. These predictions are consistent with those of the computed phase diagrams of the epitaxial PZT thin films, as presented in Figs. 5 and 6.

As discussed in the previous theoretical section, $P_1^2=P_2^2 \neq P_3^2$ for $F_{R(HT)}$ under a two-dimensional stress while $P_1^2=P_2^2=P_3^2$ in the absence of stress. Furthermore, under the condition of tensile stress, the polarization parallel to the a_1 or a_2 direction should be larger than that parallel to the a_3 direction (Fig. 1). This explains why P_1 is consistently larger than P_3 for temperatures below the F_O-$F_{R(HT)}$ transition point, as shown in Fig. 7(b). Contrary to this, a reverse trend is expected under a compressive stress, as shown in Fig. 7(c) for temperatures below the F_T-$F_{R(HT)}$ transition point.

The effects of the film stress on the temperature-dependent spontaneous polarization of the Ti-rich PZT 30/70 epitaxial thin film are summarized in Fig. 8. Irrespective of the sign of stress, the tetragonal phase becomes stable below T_C and the Curie temperature increases slightly under a two-dimensional stress. As indicated in the figure, the direction of the spontaneous polarization is parallel to the a_1 direction under a tensile stress while it is parallel to the a_3 direction under a compressive stress. All these computational results are consistent with those of the Ti-rich region of the simulated phase diagrams, as shown in Figs. 5 and 6. Besides, a comparison of the results shown in Fig. 7 with those in Fig. 8 indicates that, irrespective of the sign of film stress, a discontinuous change in the spontaneous polarization at the Curie point is much more pronounced in the Ti-rich region of the MPB (i.e., PZT 30/70). This reflects the fact that the discontinuous volume change at the P_C-F_{T3} (or F_{T1}) transition point is significantly larger than that at the P_C-$F_{R(HT)}$ transition temperature.

C. Dielectric properties

The computed dielectric susceptibility coefficients of the PZT 70/30 and 30/70 epitaxial thin films are plotted in Figs. 9 and 10, respectively, as a function of temperature. As shown in Fig. 9, there occur two consecutive ferroelectric transitions in the epitaxial PZT 70/30 under a two-dimensional film stress. They are the P_C-F_O and F_O-$F_{R(HT)}$ transitions under a tensile stress, whereas they are the P_C-F_{T3} and F_{T3}-$F_{R(HT)}$ transitions under a compressive stress.

In the presence of tensile stress, η_{11} should be much more susceptible to the P_C-F_O transition than the F_O-$F_{R(HT)}$ transition. This is because the P_C-F_O transition involves a discontinuous change in the polarization P_1 but not in P_3. On the other hand, the latter invokes a discontinuous appearance of P_3 from 0 [Fig. 7(b)] upon cooling the epitaxial film. Therefore, η_{33} should be susceptible to the F_O-$F_{R(HT)}$ transition while it is rather insensitive to the P_C-F_O transition that does not involve a change in P_3. Nevertheless, there should be an additional weak peak in η_{33} at the P_C-F_O transition point and in η_{11} at the F_O-$F_{R(HT)}$ transition temperature.

Similar arguments can be applied to an epitaxial film under a compressive stress. In this case, η_{11} should be much

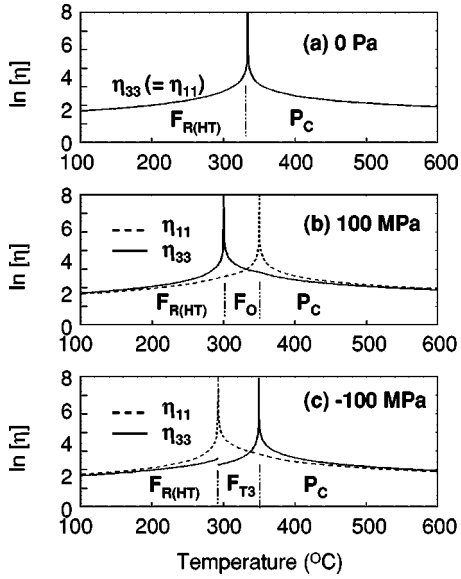

FIG. 9. Computed dielectric susceptibility of the PZT 70/30 vs temperature at three different values of two-dimensional stress: (a) 0 Pa, (b) 100 MPa, and (c) −100 MPa. All the computations are based on the original cubic P_{m3m} symmetry.

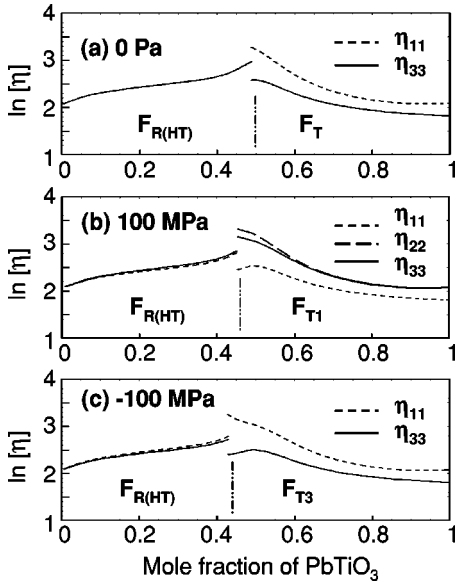

FIG. 11. Computed dielectric susceptibility of PZT solid-solution system at 25°C plotted as a function of composition at three different values of two-dimensional stress: (a) 0 Pa, (b) 100 MPa, (c) −100 MPa.

more susceptible to the F_{T3}-$F_{R(HT)}$ transition than the P_C-F_{T3} transition because the former involves a discontinuous change in the polarization P_1 (or equivalently P_2) from 0. On the other hand, η_{33} should be susceptible to the P_C-F_{T3} transition because it accompanies a discontinuous change in P_3 at the Curie point. The computational result shown in Fig. 9(c) clearly supports these conclusions. Because the F_{T3}-$F_{R(HT)}$ transition also involves a change in the direction and the magnitude of P_3, η_{33} should also be sensitive to this first-order transition. As you see in Fig. 9(c), there is a discontinuity in η_{33} at the F_{T3}-$F_{R(HT)}$ transition point.

It is interesting to notice that the dielectric susceptibility parallel to the polar axis is higher than the susceptibility perpendicular to the polar axis in the vicinity of the Curie point. However, as shown in Fig. 10, this trend is reversed as temperature decreases and goes away from the Curie point. This is caused by the ratio of $-\alpha_{12}/\alpha_{11}$ used in the phenomenological thermodynamic theory. For $BaTiO_3$ and $PbTiO_3$ systems, this reversal in the dielectric susceptibility has been studied theoretically and confirmed experimentally.[34–36] Figure 10(b) also shows that the dielectric susceptibilities for the F_{T1} phase under a tensile stress are different from each other ($\eta_{11} \neq \eta_{22} \neq \eta_{33}$). These differences are formally given in Eqs. (2.6b) and (2.7b) and are caused by the special boundary conditions related to the F_{T1} phase, as presented in Eq. (2.3b).

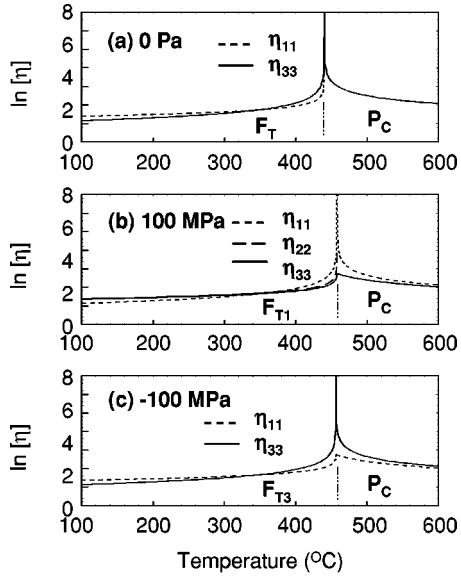

FIG. 10. Computed dielectric susceptibility of the PZT 30/70 vs temperature at three different values of two-dimensional stress: (a) 0 Pa, (b) 100 MPa, and (c) −100 MPa.

The compositional dependence of the dielectric susceptibility coefficients of the epitaxial PZT film at 25 °C is plotted in Fig. 11 for three different states of two-dimensional stress. As indicated in the figure, the MPB composition that leads to the F_T-$F_{R(HT)}$ transition at near 25 °C moves toward the rhombohedral-phase field, regardless of the sign of two-dimensional film stress. As a result of this, the dielectric susceptibility under a two-dimensional stress generally exhibits its maximum value at a newly established MPB composition (i.e., Zr/Ti>52/48).

For the susceptibility corresponding to the direction of the spontaneous polarization, however, the composition for the peak dielectric susceptibility is little changed from its original MPB composition (i.e., Zr/Ti=52/48), as shown in Fig. 11(b) for η_{11} and Fig. 11(c) for η_{33}. Under a two-dimensional compressive stress, the a_3 direction, which is the direction of the spontaneous polarization of F_{T3}, is relatively under a tensile stress. Because a tensile stress exerts along the direction of the spontaneous polarization, η_{33} is not likely to be greatly influenced by the film stress. Similar arguments can also be made for η_{11} under a two-dimensional tensile stress. All these computational results suggest that dielectric properties generally exhibit their maximum values

at a newly established Zr-rich MPB composition, except for those parallel to the direction of the spontaneous polarization that tends to align along the direction of tensile stress.

IV. CONCLUSIONS

Effects of film stresses on the phase stability and various ferroelectric properties of the epitaxially oriented $Pb(Zr,Ti)O_3$ (PZT) thin film were theoretically investigated using a two-dimensional thermodynamic model based on the Landau-Devonshire phenomenological theory. For this purpose, we defined boundary conditions relevant to various possible phases in the epitaxial PZT film, followed by the development of the elastic Gibbs functions and various theoretical relations as to ferroelectric properties.

The theoretical computation predicts an increase in the para-ferroelectric transition temperature and an enhanced thermodynamic stability of the tetragonal-phase field, irrespective of the sign of film stress (i.e., both tensile and compressive). The computation of the composition-dependent dielectric properties suggests that, irrespective of the sign of film stress, dielectric properties usually exhibit their maximum values at a Zr-rich MPB (i.e., $Zr/Ti > 52/48$), except for those parallel to the direction of tensile stress or the direction of the spontaneous polarization.

ACKNOWLEDGMENTS

This work was supported by the Korea Research Foundation (KRF) under Contract No. 1998-017-E00136 and by the Korea Institute of Science and Technology Evaluation and Planning (KISTEP) through the NRL project.

*Email address: hmjang@postech.ac.kr

[1] R.E. Cohen, Nature (London) **358**, 136 (1992).
[2] L.E. Cross, Ceram. Bull. **63**, 586 (1984).
[3] G.H. Haertling, Ferroelectrics **131**, 1 (1992).
[4] W. Cao and L.E. Cross, Phys. Rev. B **47**, 4825 (1993).
[5] B. Jaffe, W. R. Cook, Jr., and H. Jaffe, *Piezoelectric Ceramics* (Academic, New York, 1971).
[6] C.C. Chang and C.S. Tang, Sens. Actuators A **65**, 171 (1998).
[7] A. Masuda *et al.*, J. Cryst. Growth **189/190**, 227 (1998).
[8] W.-C. Shih and M.-S. Wu, IEEE Trans. Ultrason. Ferroelectr. Freq. Control **45**, 305 (1998).
[9] J.F. Scott and C.A. Araujo, Science **246**, 1400 (1989).
[10] R. Ramesh, T. Sands, and V.G. Keramidas, Mater. Sci. Eng., A **822**, 283 (1994).
[11] K. Kushida-Abdelghafar *et al.*, J. Mater. Res. **13**, 3265 (1998).
[12] O. Auciello, J.F. Scott, and R. Ramesh, Phys. Today **51** (7), 22 (1998).
[13] J. D. Olivas and S. Bolin, JOM **50**, 38 (1998).
[14] M.A. Dubois and P. Muralt, IEEE Trans. Ultrason. Ferroelectr. Freq. Control **45**, 1169 (1998).
[15] Y. Ohba, K. Arita, T. Tsurumi, and M. Daimon, Jpn. J. Appl. Phys., Part 1 **33**, 5305 (1994).
[16] D.E. Dausch and G.H. Haertling, J. Mater. Sci. **31**, 3409 (1996).
[17] S.B. Krupanidhi, N. Maffei, M. Sayer, and K. Ei-Assal, J. Appl. Phys. **54**, 6601 (1983).
[18] L. Sun *et al.*, Phys. Rev. B **55**, 12 218 (1997).
[19] Y.I. Yuzyuk *et al.*, J. Appl. Phys. **84**, 452 (1998).
[20] F. Tsai and J.M. Cowley, Appl. Phys. Lett. **65**, 1906 (1994).
[21] Y.G. Wang, W.L. Zhong, and P.L. Zhang, Phys. Rev. B **51**, 5311 (1995).
[22] S.B. Desu, Phys. Status Solidi A **141**, 119 (1994).
[23] S.B. Ren, C.J. Lu, H.M. Shen, and Y.N. Wang, Phys. Rev. B **55**, 3485 (1997).
[24] T. Kumazawa *et al.*, Appl. Phys. Lett. **72**, 608 (1998).
[25] A. Amin, R.E. Newnham, and L.E. Cross, Phys. Rev. B **34**, 1595 (1986).
[26] T. Yamamoto and Y. Makino, Jpn. J. Appl. Phys., Part 1 **35**, 3214 (1996).
[27] S.H. Oh and H.M. Jang, J. Appl. Phys. **85**, 2815 (1999).
[28] S.H. Oh and H.M. Jang, Appl. Phys. Lett. **72**, 1457 (1998).
[29] A.M. Glazer, Acta Crystallogr., Sect. B: Struct. Crystallogr. Cryst. Chem. **28**, 3384 (1972).
[30] T.R. Halemane, M.J. Haun, L.E. Cross, and R.E. Newnham, Ferroelectrics **62**, 149 (1985).
[31] D.L. Corker *et al.*, J. Phys.: Condens. Matter **10**, 6251 (1998).
[32] M.J. Haun, E. Furman, S.J. Jang, and L.E. Cross, Ferroelectrics **99**, 13 (1989); **99**, 27 (1989); **99**, 45 (1989); **99**, 55 (1989); **99**, 63 (1989).
[33] Y. Yano, K. Iijima, Y. Daltoh, T. Terashima, and Y. Bando, J. Appl. Phys. **76**, 7833 (1994).
[34] A.F. Devonshire, Philos. Mag. **40**, 1040 (1949).
[35] D. Meyerhofer, Phys. Rev. **112**, 413 (1958).
[36] M.J. Haun, E. Furman, S.J. Jang, H.A. Mckinstry, and L.E. Cross, J. Appl. Phys. **62**, 3331 (1987).